The relative compliance of energy-storing tendons may be due to the helical fibril arrangement of their fascicles

Tom Shearer

School of Mathematics, University of Manchester, Manchester, M13 9PL, United Kingdom
Tel.: +44(0)161-275-5810
Fax: N/A
E-mail: `tom.shearer@manchester.ac.uk`

Chavaunne T. Thorpe, Ewa M. Spiesz, Hazel R.C. Screen

Institute of Bioengineering, School of Engineering and Materials Science, Queen Mary University of London, Mile End Road, London E1 4NS, UK

Word count: 1557 (Max allowed for Short Communication = 2000)

Abstract

A non-linear elastic microstructural model is used to investigate the relationship between structure and function in energy-storing and positional tendons. The model is used to fit mechanical tension test data from the equine common digital extensor tendon (CDET) and superficial digital flexor tendon (SDFT), which are used as archetypes of positional and energy-storing tendons, respectively. The fibril crimp and fascicle helix angles of the two tendon types were used as fitting parameters in the mathematical model in order to predict their values. The fibril Young's modulus and collagen volume fraction were taken from the literature and the matrix shear modulus was estimated from previously collected mechanical test data. The fibril crimp angles were predicted to be $15.9^\circ \pm 2.9^\circ$ in the CDET and $17.9^\circ \pm 5.7^\circ$ in the SDFT and were not found to be statistically significantly different between the two tendon types ($p = 0.420$). The fascicle helix angles were predicted to be $8.8^\circ \pm 9.4^\circ$ in the CDET and $24.9^\circ \pm 14.2^\circ$ in the SDFT and were found to be highly statistically significantly different between the two tendon types ($p = 0.001$). This supports previous qualitative observations that helical sub-structures are more likely to be found in energy-storing tendons than in positional tendons and explains that the relative compliance of energy-storing tendons may be directly caused by these helical sub-structures.

Key words: Collagen, Mathematical modelling, Micromechanics, Non-linear elasticity, Structure-function

Nomenclature

E	fibril Young's modulus
μ	ground state shear modulus of tendon interfascicular matrix
ϕ	collagen volume fraction
θ_o	outer fibril crimp angle
α	fascicle helix angle
$\mathbf{M}$	fascicle alignment vector
λ, e	longitudinal stretch/strain
$\mathbf{F}$	deformation gradient
$\mathbf{e}_i$, $\mathbf{E}_J$	basis vectors in deformed/undeformed configuration
r, θ, z	circular cylindrical coordinates in deformed configuration
R, Θ, Z	circular cylindrical coordinates in undeformed configuration
W	strain energy function
I_1, I_4	isotropic/anisotropic strain invariant
λ^*	critical stretch at which toe-region ends
β	$2(1-\cos^3\theta_o)/(3\sin^2\theta_o)$
γ, η	constants defined in equations (5) and (6), respectively
$\mathbf{S}$	nominal stress
p	Lagrange multiplier
S_{zz}	longitudinal nominal stress
F	force in interfascicular matrix at 10% of failure load
l, A	interfascicular matrix thickness/contact area
Δx	extension of interfascicular matrix at 10% of failure load

1. Introduction

Tendons have varying mechanical requirements depending on their function. Positional tendons need to be stiff in order to keep joints in place, whereas energy-storing tendons play a role in locomotion (Alexander, 1991) and are necessarily more compliant (Lichtwark and Wilson, 2007 and Lichtwark and Wilson, 2008). This specialisation of mechanical properties between tendon types occurs despite them being composed of the same elementary materials - primarily collagen type I, which is organised into a hierarchical structure consisting of fibrous sub-units of varying diameters, each of which is interspersed with a small amount of primarily non-collagenous matrix (Kastelic et al., 1978). The fundamental building block of the collagen hierarchy is the fibril, which has a diameter of 10-20 nm and aggreagates to build fibres (diameter: 10-50 μm) and fascicles (50-400 μm). It is thought that structural and compositional differences in this hierarchy give rise to the differing mechanical properties of different tendons (Thorpe et al., 2013a, 2013b).

One approach to determine how the geometrical arrangement of tendon sub-units affects gross mechanical properties is to use mathematical modelling. Many models have been proposed over the last several decades to describe the mechanical behaviour of tendons, and soft tissues in general; however, many of these are either phenomenological, e.g. (Gou, 1970), or contain a very large number of parameters, e.g. (Limbert, 2011), some of which may be extremely challenging to measure experimentally. An overview of the approaches to tendon modelling is given in the introduction of (Shearer et al., 2016).

To avoid the problems associated with earlier approaches, two models have previously been developed (Shearer, 2015a, 2015b) with the specific aim of ensuring a microstructural basis, whilst keeping the number of necessary parameters to a minimum. The latter of these requires only two constitutive parameters and four structural quantities, namely: the collagen fibril Young's modulus E, the matrix shear modulus μ, the collagen volume fraction ϕ, the outer fibril crimp angle θ_o, the fascicle helix angle α (this term was referred to as the *fibril* helix angle in (Shearer, 2015b)) and the fascicle alignment vector $\mathbf{M}$ (see Figure 1). All of these quantities can potentially be measured via either mechanical testing (Wenger et al., 2007), histology (Screen et al., 2005) or X-ray micro-computed tomography (Shearer et al., 2014; Balint et al., 2016; Shearer et al., 2016). In the current paper, this model (Shearer, 2015b) is used to investigate the stress-strain behaviour of two types of equine tendon: one positional - the common digital extensor tendon (CDET), and one energy-storing - the superficial digital flexor tendon (SDFT). It is demonstrated that the differences in mechanical properties between the two tendon types can be explained as being entirely the result of differences in the geometical arrangement of collagen withing the fascicles as opposed to differences in their constitutive parameters. The model predicts that the SDFT is likely to have a considerably larger fascicle helix angle than the CDET - a prediction that supports previous experimental observations (Thorpe et al., 2013b).

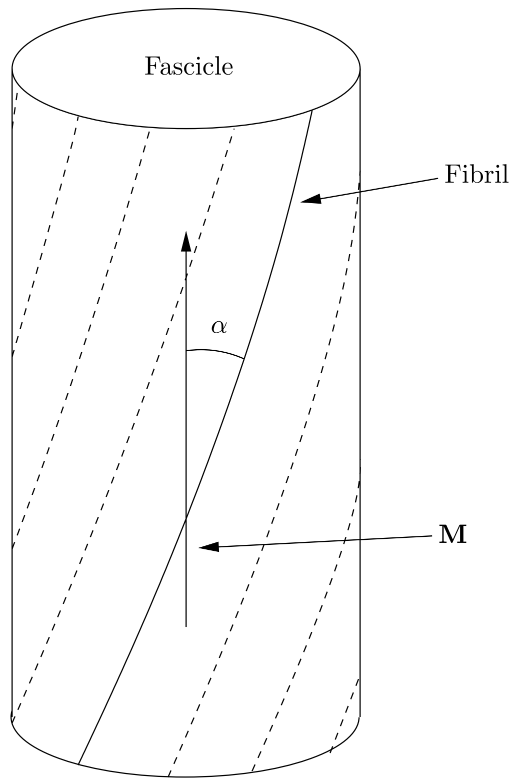

Figure 1: Diagram illustrating the fascicle helix angle α and the fascicle alignment vector $\mathbf{M}$.

Note that this diagram omits fibril crimp and instead shows the *average* fibril direction.

2. Methods

2.1. Mechanical testing

The mechanical test data were collected for a previous study (Thorpe et al., 2012) and the testing protocol is described in detail therein. Briefly, the CDET and SDFT were dissected from the left forelimbs of 18 horses aged 3-20 years and frozen until the day of testing. On the day of testing, tendons were thawed and their cross-sectional areas were measured, as described ny (Goodship and Birch, 2005). The tendons were mounted vertically in a servo-hydraulic materials testing machine (Dartec Ltd., Stroubridge, UK) with a 50 kN load cell and were gripped with cryoclamps cooled by liquid carbon dioxide (Riemersa and Schamhardt, 1982). They were pre-loaded to 25 N (CDET) or 100 N (SDFT) and were subjected to 20 preconditioning cycles between 0% and 5.25% strain at a frequency of 0.5 Hz, using a protocol adapted from (Batson et al., 2003). The load was then removed so that slack was visible in the tendons, which were then tested to failure at a rate of 5%/s. The stresses in the tendons were recorded as forces per unit undeformed areas, so that the reported values are nominal stresses, and the displacements at which the initial pre-loads were reached were taken as the start points for the tests in all specimens.

2.2. Mathematical modelling

Each tendon is modelled as an incompressible, transversely isotropic, non-linear elastic cylinder, subjected to a longitudinal stretch λ (≥ 1), so that the deformation gradient is given by (Shearer, 2015b)

$$\mathbf{F} = F_{iJ}\mathbf{e}_i \otimes \mathbf{E}_J, \qquad F_{iJ} = \begin{pmatrix} \lambda^{-\frac{1}{2}} & 0 & 0 \\ 0 & \lambda^{-\frac{1}{2}} & 0 \\ 0 & 0 & \lambda \end{pmatrix}, \tag{1}$$

where $\mathbf{e}_i$, $i = (r, \theta, z)$, and $\mathbf{E}_J$, $J = (R, \Theta, Z)$, are deformed and undeformed unit vectors in the radial, azimuthal and longitudinal directions, respectively. The longitudinal stretch is related to the longitudinal strain e via $\lambda = 1 + e$. To calculate the theoretical nominal stresses, the strain energy function from (Shearer, 2015b) is utilised:

$$W = (1-\phi)\frac{\mu}{2}(I_1 - 3), \qquad I_4 < 1, \tag{2}$$

$$\begin{aligned} W = (1-\phi)\frac{\mu}{2}(I_1 - 3) + \phi\frac{E}{3\sin^2\theta_o}\Bigg(2\cos\alpha\sqrt{I_4} - \\ 3\log\left(2\left(\cos^2\alpha\sqrt{I_4} + \cos\alpha\sqrt{\sin^2\alpha + I_4\cos^2\alpha}\right)\right) + \\ \frac{\cos\alpha\sqrt{I_4}}{\sin^2\alpha\sqrt{\sin^2\alpha + I_4\cos^2\alpha}}\Bigg) + \gamma, \qquad 1 \leq I_4 \leq \lambda^{*2}, \end{aligned} \tag{3}$$

$$\begin{aligned} W = (1-\phi)\frac{\mu}{2}(I_1 - 3) + \phi E\Bigg(\beta\cos\alpha\sqrt{I_4} - \\ \log\left(\cos^2\alpha\sqrt{I_4} + \cos\alpha\sqrt{\sin^2\alpha + I_4\cos^2\alpha}\right)\Bigg) + \eta, \qquad I_4 > \lambda^{*2}, \end{aligned} \tag{4}$$

where I_1 and I_4 are strain invariants as defined in (Holzapfel and Ogden, 2010), for example, $\lambda^* = 1/\cos\alpha\sqrt{1/\cos^2\theta_o - \sin^2\alpha}$ is the critical stretch at which the toe-region ends (Shearer, 2015b), $\beta = 2(1 - \cos^3\theta_o)/(3\sin^2\theta_o)$,

$$\gamma = -\frac{E}{3\sin^2\theta_o}\left(2\cos\alpha - 3\log\left(\cos^2\alpha + \cos\alpha\right) + \frac{\cos\alpha}{\sin^2\alpha}\right), \tag{5}$$

and

$$\eta = \gamma + E\left(\left(\frac{\cos\theta_o}{\sin^2\theta_o}\frac{1}{\sin^2\alpha} + \frac{2}{\sin^2\theta_o} - 3\beta\right)\sqrt{\frac{1}{\cos^2\theta_o} - \sin^2\alpha} \right.$$
$$\left. -3\frac{\cos^2\theta_o}{\sin^2\theta_o}\log\left(\cos\alpha\left(\frac{1}{\cos\theta_o} + \sqrt{\frac{1}{\cos^2\theta_o} - \sin^2\alpha}\right)\right)\right). \quad (6)$$

Equations (1)–(4) can be substituted into the general equation for the nominal stress in a transversely isotropic non-linear elastic material, which, for a strain energy function that is only dependent on I_1 and I_4 is given by:

$$\mathbf{S} = -p\mathbf{F}^{-1} + 2W_1\mathbf{F}^{\mathrm{T}} + 2W_4\mathbf{M}\otimes\mathbf{FM}, \quad (7)$$

where p is a Lagrange multiplier associated with the incompressibility constraint, $W_i = \partial W/\partial I_i$ and, $\mathbf{M}$ is a unit vector oriented in the direction of the fascicles in the undeformed configuration. It is assumed that the fascicles are coaligned with the longitudinal axis of the tendon in both the CDET and SDFT, so that $\mathbf{M} = \mathbf{E}_Z$. In reality, this is not the case; however, it is assumed that the deviation from longitudinal alignment is small enough to be negligible.

Upon applying stress-free boundary conditions on the curved surface of the cylinder, thus determining the value of p, the following expression is obtained for the longitudinal nominal stress:

$$S_{zz} = \begin{cases} (1-\phi)\mu(\lambda - \lambda^{-2}) + \phi\dfrac{E\cos\alpha}{3\sin^2\theta_o}\times \\ \left(2 - \dfrac{3}{\sqrt{\sin^2\alpha + \lambda^2\cos^2\alpha}} + \dfrac{1}{(\sin^2\alpha + \lambda^2\cos^2\alpha)^{\frac{3}{2}}}\right), & 1 \le \lambda \le \lambda^*, \\ (1-\phi)\mu(\lambda - \lambda^{-2}) + \\ \qquad \phi E\cos\alpha\left(\beta - \dfrac{1}{\sqrt{\sin^2\alpha + \lambda^2\cos^2\alpha}}\right), & \lambda > \lambda^*. \end{cases} \quad (8)$$

This expression is used to model the mechanical test data obtained for the CDET and SDFT.

2.3. Parameter selection

In order to fit equation (8) to the experimental data, it is necessary to select values for the constitutive parameters in the model.

2.3.1. Constitutive parameters

For the collagen Young's modulus, there is a wide range of reported values in the literature, ranging from 32 MPa (Graham et al., 2004) to 12 GPa (Eppell et al., 2006). To the authors' knowledge there is no data available for equine collagen fibrils; therefore, bovine data was used as a substitute - the value selected here was 1.9 GPa, which is the value reported by Grant et al. (2008) for bovine collagen fibrils under ambient conditions.

A lack of data is available in the literature for the matrix shear modulus due to the difficulties involved in measuring it experimentally; therefore, a custom method was developed to estimate the values of this parameter in the CDET and SDFT based on mechanical test data from a previous study (Thorpe et al., 2012). The testing protocol is decribed in detail within that paper; however, briefly, groups of two fascicles bound together by the interfascicular matrix were dissected from the CDET and SDFT (n=17, 12 samples per tendon). The fascicles were secured into a custom-made dissection rig and the opposing end of each fascicle was cut transversely, leaving 10mm of intact interfascicular matrix. The intact end of each fascicle was then secured in a materials testing machine and pulled apart to failure at a speed of 1 mm/s. Force and extension data were recorded and the point at which a load of 0.02N was reached was defined as the test start point. The matrix shear modulus was then estimated using the following equation:

$$\mu = \frac{Fl}{A\Delta x}, \tag{9}$$

where F is the force and Δx is the extension in the matrix at 10% of the failure load, l is its thickness and A is its contact area. The contact area was estimated by multiplying the average fascicle diameter by the test length (10mm). The thickness was estimated based on values calculated by Ali et al. (2015). Using this method, it was estimated that the matrix shear modulus of the CDET is 1.01 kPa and of the SDFT is 1.62 kPa.

2.3.2. Structural parameters

For the collagen volume fraction, an estimate was made based on the collagen area fractions reported in (Screen et al., 2005) for nonincubated rat tail tendon - the selected value was 0.8. The fibril crimp and helix angles were used as fitting parameters in order to predict their values. The function (8) was used to fit each of the experimental data sets up to 10% strain, beyond which it was assumed that the deformation was no longer elastic. The experimental data was fitted using the *NonlinearModelFit* command in *Mathematica 9.0* (Wolfram Research, Inc., Champaign, Illinois, 2008) subject to the constraints $0 \leq \theta_o \leq 90°$ and $0 \leq \alpha \leq 90°$.

Tendon	Crimp angle (θ_o)	Helix angle (α)
CDET	$15.9° \pm 2.9°$	$8.8° \pm 9.4°$
SDFT	$17.9° \pm 5.7°$	$24.9° \pm 14.2°$

Table 1: Predicted fibril crimp and helix angles.

3. Results

The predicted fibril crimp and fascicle helix angles according to the model fit are listed in table 1 (given as mean ± standard deviation) and an example fit to the experimental data is plotted in figure 2 (plots of all 18 fits are provided in supplementary material). The minimum coefficient of determination (R^2 value) across all 36 data sets was 0.979. There was no statistically significant difference between the crimp angles of the CDET and SDFT ($p = 0.420$); however, there was a highly statistically significant difference between the helix angles of the CDET and SDFT ($p = 0.001$) according to the Mann-Whitney test.

4. Discussion

The fitting process predicted a much larger fascicle helix angle in the SDFT than in the CDET. These predictions agree with the qualitative observations in (Thorpe et al., 2013b) and support the hypothesis that helical substructures are more likely to be found in energy-storing tendons than in positional tendons. The model also provides a link between the microstructures and mechanical functions of these tendons, explaining that the relative compliance of energy-storing tendons is caused directly by the helical fibril arrangement of

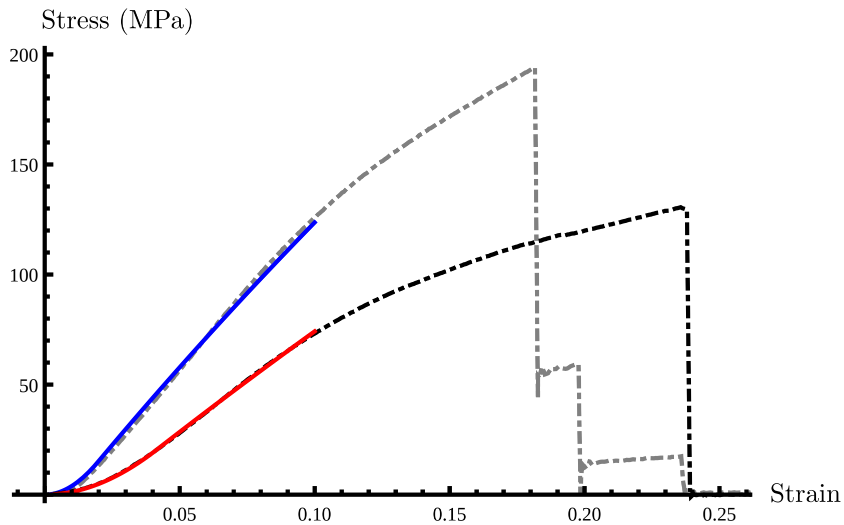

Figure 2: Example experimental (dashed) and theoretical (solid) stress-strain curves for the CDET (grey/blue) and SDFT (black/red).

their fascicles, and *not* by differences in their fibril Young's modulus or crimp angles.

Whilst different values of the matrix shear modulus were used to model each tendon, this does not affect the conclusions above as the stress in the matrix at 10% strain was 0.0001% of the total stress in the tendon on average and therefore the contribution of this phase was not important compared to that of the fibrils. The modelling was repeated three times with the same matrix shear modulus being used for both the CDET and SDFT using the values: μ =1.01 kPa, μ =1.62 kPa and μ =10 kPa. In all three cases, the predicted helix and crimp angles differed from those reported in table 1 by less than 0.01°.

Acknowledgements

TS acknowledges funding for this work from the EPSRC through Grant EP/L017997/1.

Data statement

TBC.

References

[1] Alexander, R.M., 1991. Energy-saving mechanisms in walking and running. J. Exp. Biol. 160, 55–69.

[2] Ali, O.J., Comerford, E., Canty-Laird, E., Clegg, P.D. Three-dimensional anatomy of equine superficial digital flexor tendon. Bone Joint J. 97-B(SUPP 11).

[3] Balint, R., Lowe, T., Shearer, T., 2016. Optimal contrast agent staining of ligament and tendons for X-ray computed tomography. PLoS ONE 11, e0153552.

[4] Batson, E.L., Paramour, R.J., Smith, T.J., Birch, H.L., Patterson-Kane, J.C., Goodship, A.E., 2003. Are the material properties and matrix composition of equine flexor and extensor tendons determined by their functions? Equine Vet. J. 35, 314–318.

[5] Eppell, S.J., Smith, B.N., Kahn, H., Ballarini, R., 2006. Nano measurements with micro-devices: mechanical properties of hydrated collagen fibrils. J. R. Soc. Interface 3, 117–121.

[] Goodship, A.E., Birch, H.L., 2005. Cross sectional area measurement of tendon and ligament in vitro: a simple, rapid, non-destructive technique. J. Biomech. 38, 605–608.

[6] Gou, P.-F., 1970. Strain energy function for biological tissues. J. Biomech. 3, 547–550.

[7] Graham, J.S., Vomund, A.N., Phillips, C.L., Gradnbois, M., 2004. Structural changes in human type I collagen fibrils investigated by force spectroscopy. Exp. Cell Res. 299, 335–342.

[8] Grant, C.A., Brockwell, D.J., Radford, S.E., Thomson, N.H., 2008. Effects of hydration on the mechanical response of individual collagen fibrils. Appl. Phys. Lett. 92, 233902.

[9] Holzapfel, G.A., Ogden, R.W., 2010. Constitutive modelling of arteries. Proc. R. Soc. A 455, 1551–1597.

[10] Kastelic, J. Galeski, A., Baer, E., 1978. The multicomposite structure of tendon. Connect. Tissue Res. 6, 11–23.

[11] Lichtwark, G.A., Wilson, A.M., 2007. Is Achilles tendon compliance optimised for maximum muscle efficiency during locomotion? J. Biomech. 40, 1768–1775.

[12] Lichtwark, G.A., Wilson, A.M., 2008. Optimal muscle fascicle length and tendon stiffness for maximising gastrocnemius efficiency during human walking and running. J. Theor. Biol. 252, 662–673.

[13] Limbert, G., 2011. A mesostructurally-based anisotropic continuum model for biological soft tissues Decoupled invariant formulation. Journal of the Mechanical Behavior of Biomedical Materials 4, 1637–1657.

[14] Riemersa, D.J., Schamhardt, H.C., 1982. The cyro-jaw. a clamp designed for in vitro rheology studies of horse digital flexor tendons. J. Biomech. 15, 619–620.

[15] Screen, H.R.C., Shelton, J.C., Chhaya, V.H., Kayser, M.V., Bader, D.L., Lee, D.A., 2005. The influence of noncollagenous matrix components on the micromechanical environment of tendon fascicles. Annals of Biomedical Engineering 33, 1090–1099.

[16] Shearer, T., 2015a. A new strain energy function for the hyperelastic modelling of ligaments and tendons based on fascicle microstructure. J. Biomech. 48, 290–297.

[17] Shearer, T., 2015b. A new strain energy function for modelling ligaments and tendons whose fascicles have a helical arrangement of fibrils. J. Biomech. 48, 3017–3025.

[18] Shearer, T., Bradley, R.S., Hidalgo-Bastida, A., Sherratt, M.J., Cartmell, S.H., 2016. 3D visualisation of soft biological structures by microCT. J. Cell Sci., accepted for publication.

[19] Shearer, T., Parnell, W.J., Lynch, B., Allain, J.-M., Abrahams, I.D., 2016. Sequential straightening and loading viscoelasticity: A model of the time-

dependent behaviour of tendon fascicles incorporating fibril recruitment. Proc. Roy. Soc. A., under review.

[20] Shearer, T., Rawson, S., Castro, S.J., Balint, R., Bradley, R.S., Lowe, T., Vila-Comamala, J., Lee, P.D., Cartmell, S.H., 2014. X-ray computed tomography of the anterior cruciate ligament and patellar tendon. Muscles Ligaments Tendons J. 4, 238–244.

[21] Thorpe, C.T., Udeze, C.P., Birch, H.L., Clegg, P.D., Screen, H.R.C., 2012. Specialization of tendon mechanical properties results from interfascicular differences. J. R. Soc. Interface 9, 3108–3117.

[22] Thorpe, C.T., Birch, H.L., Clegg, P.D., Screen, H.R.C., 2013a. The role of the non-collagenous matrix in tendon function. Int. J. Exp. Path. 94, 248–259.

[23] Thorpe, C.T., Klemt, C., Riley, G.P., Birch, H.L., Clegg, P.D., Screen, H.R.C., 2013b. Helical sub-structures in energy-storing tendons provide a possible mechanism for efficient energy storage and return. Acta Biomater. 9, 7948–7956.